Chapter

Effect of Zr Addition and Aging Treatment on the Tensile Properties of Al-Si-Cu-Mg Cast Alloys

Jacobo Hernandez-Sandoval, Mohamed H. Abdelaziz, Agnes M. Samuel, Herbert W. Doty and Fawzy H. Samuel

Abstract

The present study focused on the tensile properties at ambient and high temperatures of alloy 354 without and with the addition of zirconium. Tensile tests were performed on alloy samples submitted to various aging treatments, with the aim of understanding the effects of the addition made on the tensile properties of the alloy. Zirconium reacts only with Ti, Si, and Al in the alloys examined to form the phases $(Al,Si)_2(Zr,Ti)$ and $(Al,Si)_3(Zr,Ti)$. Testing at 25°C reveals that the minimum and maximum quality index values, 259 and 459 MPa, are observed for the as-cast and solution heat-treated conditions, respectively. The yield strength shows a maximum of 345 MPa and a minimum of 80 MPa within the whole range of aging treatments applied. The ultimate tensile and yield strength values obtained at room temperature for T5-treated samples stabilized at 250°C for 200 h are comparable to those of T6-treated samples stabilized under the same conditions, and higher in the case of elevated-temperature (250°C) tensile testing. Coarsening of the strengthening precipitates following such prolonged exposure at 250°C led to noticeable reduction in the strength values, particularly the yield strength, and a remarkable increase in the ductility values.

Keywords: aluminum alloys, aging, thermal exposure, tensile testing, precipitation, fractography

1. Introduction

The 354 alloy belongs to the Al-Si-Cu-Mg system similar to B319 alloy that is widely used for automotive engine blocks [1]. The high silicon content in the 354 alloy improves the alloy castability whereas the presence of Cu and Mg noticeably enhances the yield strength (YS) and the ultimate tensile strength (UTS) of the 354 alloy due to the formation of intermetallic phases, mainly Al_2Cu or eutectic Al + Al_2Cu, and Mg_2Si precipitates [2, 3]. However, segregation behavior of Cu may lead to incipient melting during solution treatment which will apparently reduce the alloy strength [4]. Addition of Mg has a strong affinity to react with Sr, leading to the formation of a complex $Mg_2SrAl_4Si_3$ intermetallic phase, and hence reducing the effectiveness of Sr as a Si modifying agent [5]. In the absence of Cu, high Fe and Mg contents lead to the formation of π-$FeMg_3Si_6Al_8$ phase which is difficult to dissolve during the solution

treatment process [6, 7]. In the quaternary Al-Si-Cu-Mg alloy system, *Q*-phase ($Al_4Mg_8Cu_2Si_6$) can coexist with the Al_2Cu, Mg_2Si, and Si phases depending on the levels of Cu, Mg, and Si [8–11]. The different factors that may influence the mechanical behavior of cast aluminum alloys are schematically represented in **Figure 1** [12].

Zirconium may be added to Al alloys in order to refine the grain structure due to the presence of fine coherent dispersoids (mainly Al_3Zr) which obstruct dislocation motion and in turn, enhance the elevated temperature mechanical properties of aluminum alloys [13]. In order to increase the volume fraction of Al_3Zr precipitates and based on the phase diagram of Al-Zr, the concentration of Zr in the alloys investigated in this study was kept at around 0.3 wt.% [14].

The main purpose of solution heat treatment is to obtain a supersaturated solid solution at high temperatures (below the eutectic temperature). As a result, a homogeneous supersaturated solid solution (SSSS) will form through dissolving the precipitated phases during the solidification process, such as β-Mg_2Si, θ-Al_2Cu, Q-$Al_5Cu_2Mg_8Si_6$, π-$Al_9FeMg_3Si_5$ and β-Al_5FeSi phases. The β-Mg_2Si and θ-Al_2Cu phases can be easily dissolved when the optimum solution heat treatment temperature and time are employed. The solution treatment temperature is determined according to the alloy composition and solid solubility limit; however, it must be lower than the melting point of the phases that exist in the as-cast structure to avoid incipient melting of these phases [15, 16].

Following the empirically developed concept of quality index proposed by Drouzy et al. [17, 18] Cáceres proposed a mathematical model emphasizing the significance of the quality index as follows [17, 19, 20]:

$$Qc = \left[(qn)^n \, exp^{-qn} + 0.4 log\,(100qn) \right] \tag{1}$$

where quality index *Q* can be calculated using the relative quality index (q), strain-hardening exponent (n), and the strength coefficient (K).

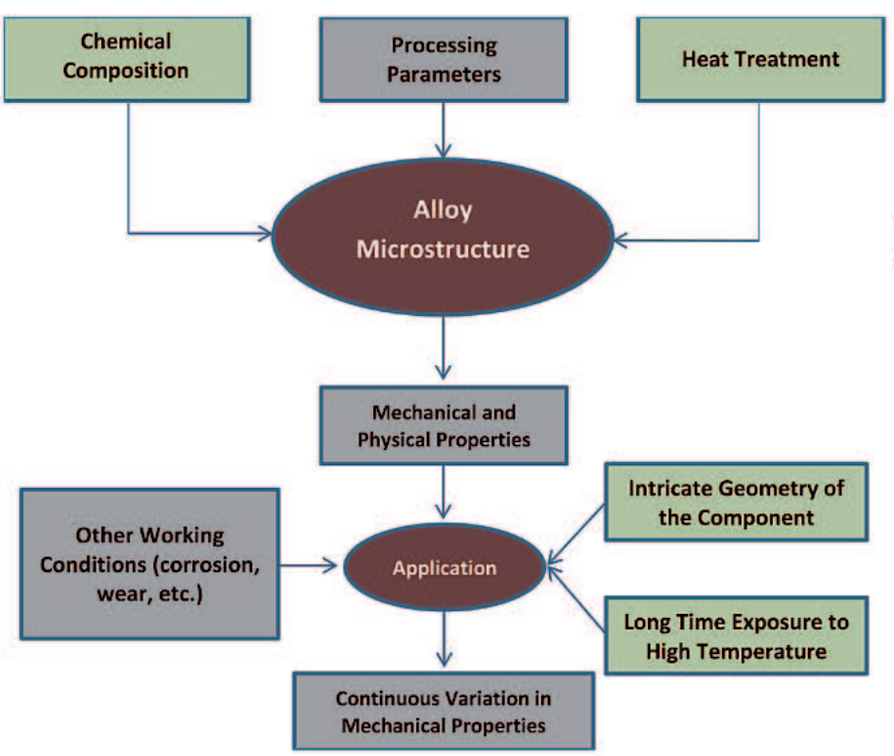

Figure 1.
Schematic representation of factors affecting alloy performance [12].

The present study was undertaken to explore the effect of Zr addition and aging conditions of the as cast tensile bars on:

1. Characterizing the microstructural features of the investigated alloys,

2. Exploring the tensile properties at both ambient and elevated temperatures, and

3. Correlating the tensile properties to the microstructural features to establish the strengthening or softening mechanisms responsible for the observed properties.

It should be noted here that the term "temperature" applies to aging temperatures as well as testing temperature.

2. Experimental procedure

Alloy 354 modified with 200 ppm of strontium (using Al-10% Sr master alloy) and grain refined using 0.20 wt.%Ti (Al-5%Ti-1%B) was used as the base alloy (alloy A). To this alloy, 0.3%Zr in the form of Al-25wt.%Zr master alloy was added (alloy B). The chemical compositions of both alloys are listed in **Table 1**. **Figure 2** shows the microstructure of the as-received base alloy ingots. Melting and casting procedures were carried out as described elsewhere.

Alloy code	Element (wt.%)								
	Si	Fe	Cu	Mn	Mg	Zr	Ti	Sr	Al
A	9.1	0.12	1.8	0.0085	0.6	—	0.18	0.02	87.6
B	9.1	0.12	1.8	0.0085	0.6	0.3	0.18	0.02	87.6

Table 1.
Chemical composition of the 354 alloys used in this study.

Figure 2.
Microstructure (200×) of the base alloy 354 used in this work.

To prepare test bars for the tensile tests, three samples for chemical analysis were also taken at the time of the casting; this was done at the beginning, in the middle, and at the end of the casting process to ascertain the exact chemical composition of each alloy. The experimental work was divided into two stages: Stage I in which the 354 alloy (alloy A) was used, and Stage II where the 354 alloy with 0.3%Zr (alloy B) was used. In Stage I, the melt temperature was kept around 750°C, whereas in Stage II, the melt temperature was superheated to 800°C, to ensure the complete decomposition of the Al-25%Zr master alloy used.

2.1 Stage I-alloy A

Tensile bars were solution heat treated at 495°C for 8 h, followed by quenching in warm water at 60°C, after which artificial aging was applied according to the plan listed in **Table 2**. After aging, the test bars were allowed to cool naturally at room temperature (25°C). All of the samples, whether as-cast, solution heat-treated, or aged, were tested to the point of fracture using an MTS servo-hydraulic mechanical testing machine at a strain rate of 4×10^{-4} s^{-1}.

The yield strength (YS) was calculated according to the standard 0.2% offset strain, and the fracture elongation was calculated as the percent elongation (%El) over 50 mm gauge length, as recorded by the extensometer. The ultimate tensile strength (UTS) was also obtained from the data acquisition system of the MTS machine. The average %El, YS, or UTS values obtained from the five samples tested per condition were considered to be the values representing that specific condition. An extensometer, or strain gage was used in the tests to measure the extent of deformation in the samples.

Samples for metallography were sectioned from the tensile-tested bars of all the alloys studied, about 10 mm below the fracture surface. The percentage porosity and eutectic Si-particle characteristics were measured and quantified using an optical microscope linked to a Clemex image analysis system. The microstructures of the polished sample surfaces were examined using an Olympus PMG3 optical microscope. Phase identification was carried out using electron probe microanalysis (EPMA) in conjunction with wavelength dispersive spectroscopic (WDS) analysis, using a JEOL*JXA-889001WD/ED combined microanalyzer operating at 20 kV and 30 nA, where the electron beam size was ~2 μm.

Mapping of certain specific areas of the polished sample surfaces was also carried out where required, so as to show the distribution of different elements within the phases. The fracture surfaces of tensile-tested samples were also examined using the same SEM, employing the backscattered electron (BSE) detector and EDS system. The fracture behavior was analyzed using the backscattered electron (BSE) images

Temperature (°C)	Aging time (h) and aging condition codes												
	2	**4**	**6**	**8**	**10**	**12**	**16**	**20**	**24**	**36**	**48**	**72**	**100**
155	1	2	3	4	5	6	7	8	9	10	11	12	13
170	14	15	16	17	18	19	20	21	22	23	24	25	26
190	27	28	29	30	31	32	33	34	35	36	37	38	39
240	40	41	42	43	44	45	46	47	48	49	50	51	52
300	53	54	55	56	57	58	59	60	61	62	63	64	65
350	66	67	68	69	70	71	72	73	74	75	76	77	78

Table 2.
Artificial aging conditions used for room temperature tension tests.

obtained, and analysis of the EDS spectra of phases observed on the fracture surface. Differential scanning calorimetry (DSC) was used to characterize the sequence of reactions occurring during the heating and/or cooling cycles of an alloy sample during a DSC scan which continuously changes with the increasing or decreasing temperature cycle to produce peaks according to the two expected reactions:

- Phase formation → heat emission → exothermic peak

- Phase dissolution → heat absorption → endothermic peak

2.2 Stage II-alloy B

For the high temperature tensile tests, samples from selected conditions were tested to fracture using an Instron Universal mechanical testing machine at a strain rate of 4×10^{-4} s^{-1}. The heating furnace installed on the testing machine is an electrical resistance, forced-air box type, having the dimensions 30 × 43 × 30 cm. The yield strength (YS) was calculated according to the standard 0.2% offset strain, and the fracture elongation was calculated as the percent elongation (%El) over the 25.4 mm gauge length as recorded by the extensometer. The ultimate tensile strength (UTS) was obtained from the data acquisition system of the universal machine. In order to reach and stabilize the intended test temperature during the tests, at the time that the samples were mounted in the tensile machine, the furnace was already pre-set at the required temperature; also, these samples were kept mounted in the furnace of the tensile testing machine for 30 min before the start of every test.

3. Results and discussion

3.1 Stage I-alloy A

Figure 3 shows the macrostructure revealing the grain size for alloy A, about 200 μm. A complete modification of the silicon particles in the microstructure of alloy A in the as-cast condition can be seen in **Figure 4(a)**. From **Figure 4(a)** and **(b)**, solution heat treatment has changed the morphology of the silicon particles from faceted to globular. As a consequence of solution heat treatment, there may also be observed a reduction in the number of silicon particles and a reduction in the density of the silicon phase, due to the diffusion of silicon into the aluminum matrix. The white arrows in **Figure 4(a)** show the rounded shape of the dendrites with grain refining [21], whereas **Figure 4(b)** reveals the dissolution of the Al_2Cu phase observed in **Figure 4(a)**—circled.

Zhu and Liu [22] proposed a model of the granulation of unmodified eutectic Si composed of three major stages during heat treatment: (i) the mass transport of solute, (ii) a discontinuous phase fragmentation, and lastly (iii) spheroidization. During heat treatment, the silicon atoms in the matrix at the Si particle tips diffuse to locations on the curved surfaces of the particles, leading to the dissolution of eutectic silicon at the tips. This transport of silicon atoms ultimately causes the fragmentation and spheroidization of eutectic silicon which is important from strength point of view compared to Si particles with sharp edges which act as sites for stress concentration.

The values of secondary dendrite arm spacing (SDAS), porosity, modification level, and grain size for both the as-cast (AC) and solution heat-treated (SHT) condition are listed in **Tables 3** and **4**. As can be seen, SHT resulted in (i) no noticeable change in both the SDAS and grain size, (ii) a significant decrease in the particle density due to coarsening of the eutectic Si particles, and (iii) almost

complete solubility of Al_2Cu in the aluminum matrix. Since the solutionizing temperature was well below the incipient melting temperature, tensile test bars revealed negligible change in the amount of porosity, i.e., no incipient melting.

Figure 3.
Macrograph showing grain size of the tensile bars in the as-cast condition.

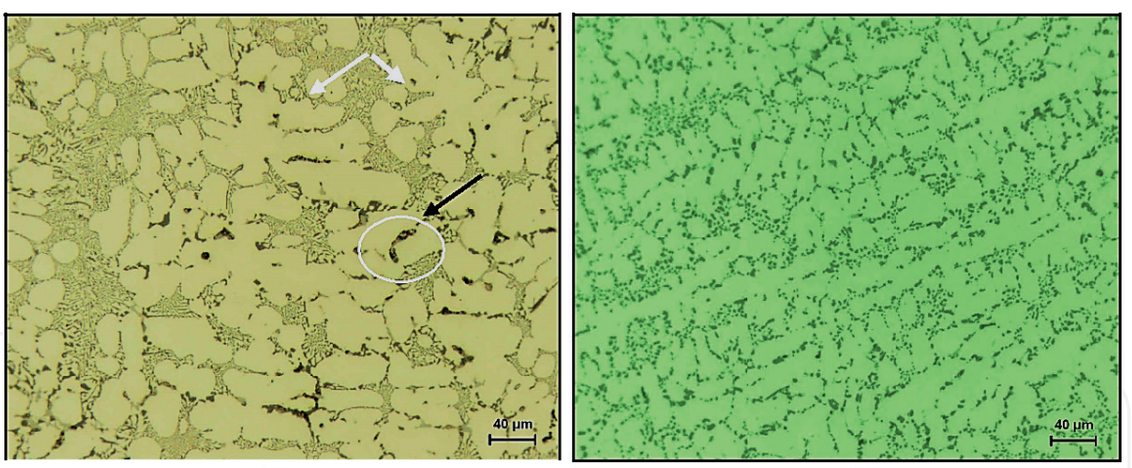

Figure 4.
Optical microstructure: (a) before, and (b) after solution heat treatment.

Alloy code condition	SDAS (µm)	Grain size (µm)	Porosity (%)		Volume fraction of intermetallics (%)	
					EPMA	
	Av*		Av	SD**	Av	SD
A-AC	19.3	201	0.14	0.06	3.08	0.32
A-SHT	23.1	192	0.12	0.05	1.27	0.10

*Average.
**Standard deviation.

Table 3.
SDAS, porosity%, grain size, level of modification, and volume fraction of intermetallics for alloy A.

Alloy code condition	Area (%)	Particle length (μm)		Roundness ratio (%)		Aspect ratio		Density (particles/mm^2)
	Av	Av	SD	Av	SD	Av	SD	
A-AC	14.58	3.522	3.94	0.4302	0.181	2.033	0.8609	39110
A-SHT	10.868	4.286	3.144	0.554	0.1547	1.641	0.5429	12080

Table 4.
Silicon particle characterization for alloy A.

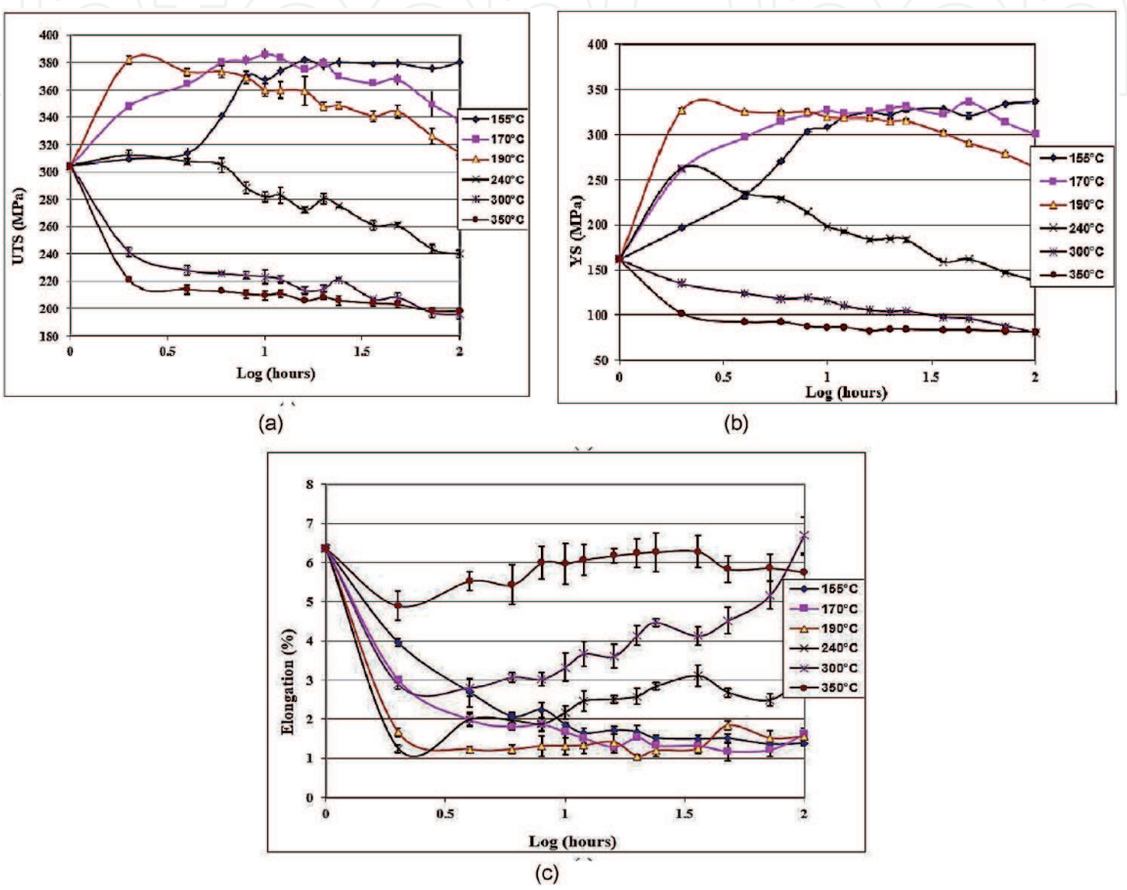

Figure 5.
Variation in alloy tensile parameters as a function of aging temperature and time: (a) UTS, (b) YS, and (c) %El.

Figure 5 illustrates the effect of aging treatment on the alloy strength parameters. The main observations inferred from this figure can be summarized as follows:

1. Solution heat treatment and artificial aging at 190°C for 2 h or at 155°C for 100 h resulted in an increase in the alloy strength by ~64% over its as-cast strength.

2. Aging at 155 or 170°C for a long period of time offered maximum resistance to softening.

3. The greatest decrease in tensile strength occurred at 240°C (312 MPa at 2 h to 240 MPa at 100 h). Similarly, a significant decrease in strength took place upon aging at 190°C for a lengthy time (from 382 MPa at 2 h to 314 MPa at 100 h) indicating the end of peak-aging or the commencement of over aging.

4. The greatest reduction in the alloy UTS and YS levels resulted when the tensile bars were aged at a temperature as high as 350°C even for a short period of 2 h.

5. In comparison to the ascendant and steady strength curves corresponding to aging temperatures of 155°C and 170°C, fluctuations in the strength curves were observed at aging temperatures of 190°C and over, similar to that reported by Reif [23] where a similar alloy was used and an ascendant monotonic strength curve was observed at an aging temperature of 155°C.

6. Although the highest ductility values were obtained after 2 h aging at 350°C (~5%), none of the aging conditions reached the higher ductility values exhibited by the solution heat-treated condition (~6.5%). This observation may be considered evidence that the mechanical behavior displayed by alloy A is common to that of the Al-Si-Cu-Mg alloys whose strength is obtained at the expense of ductility [24, 25].

In order to analyze the alloy quality by means of the Quality Index charts, the as-cast and the solution heat treated conditions plus aging conditions at 155°C, 190°C, and 350°C for aging times in the range of 2–100 h were used. From a previous study [5], K was calculated as 500 MPa.

The plastic strain and the quality index (Q) both exhibit a great improvement following solution heat treatment. The fact that plastic deformation (q) was about 0.31 in the solution-treated condition means that the alloy reached 31% of its maximum quality index value (Q). The importance of q is that it shows how much a sample is away from its maximum possible ductility q = 1 and indicates that it would be possible to control the microstructure, for example by reducing the SDAS, or the porosity, or intermetallic level to enhance the alloy ductility and hence, the quality index, Q. When the ductility increases sharply from the as-cast to the solution heat treated condition, such changes can be related to the spheroidization of silicon particles and to the uniformity of the microstructure in the solution heat-treated condition, as shown in **Figure 6(a)**.

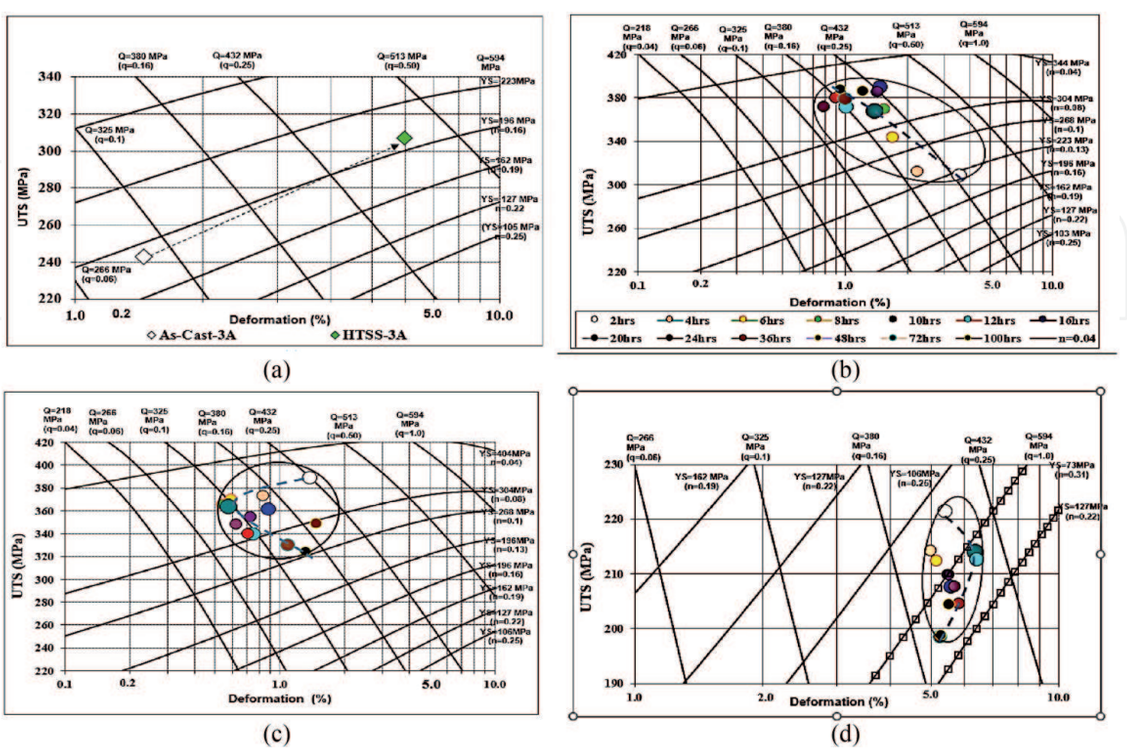

Figure 6.
Q-charts following: (a) SHT, (b) aging at 155°C, (c) aging at 190°C, and (d) aging at 350°C. Legends in (b) apply for other charts. The curved lines indicate the passage from 2 to 10 to 100 h.

From the data presented in **Figure 6(b)–(d)**, it is evident that the change in crystallographic structure of Al_2Cu phase from G-P zones (155°C) to a metastable phase (190°C) to a stable phase (350°C) is the main parameter controlling the alloy performance quality. As can be seen, at each aging temperature, all points fall within a narrow circle due the progress in the formation of the precipitated phase. The broken lines in these figures show the change in the *Q*-level as a function of aging temperature. The width of the circle deceased from 175 MPa (155°C) to 75 MPa (190°C) to 25 MPa (350°C), representing the hardening and softening behavior of the alloy as a function of the aging temperature and time [26]. Using aging times of 2 and 100 h as reference points, the *Q*, UTS and %El values are presented in **Table 5**. As can be seen, the *Q* values after 2 h are more-or-less same over such a large range of aging temperatures, due to the variation in both UTS and %El. However, aging for 100 h revealed highest value at 190°C compared to 155°C (under aging) and 350°C (over aging). The *Q* values for test bars aged at 350°C for 100 h is the same due to the balance between UTS and %El.

3.2 Stage II-alloy B

The heat treatment procedures followed for the alloy B are listed in **Table 6**. The same treatments were applied for both 25°C and 250°C tensile testing.

Figure 7 [27] shows the DSC heating curves of the alloys in the as-cast and SHT conditions, where three explicit peaks could be detected and coded 1, 2, 3. Considering the main parameter is the precipitation of Al_2Cu phase particles, thus the height of peak number 1 following SHT compared to that in the as-cast condition plays a crucial role in controlling the alloy performance after aging. In addition, it is an indication of the effectiveness of the SHT process in dissolving the initial Al_2Cu phase. In **Figure 7**, peak # 1 after solutionizing is more

Aging temperature (°C)	*Q* (MPa)	UTS (MPa)	%El	Aging time (h)
155	432	300	3.5	2
190	432	388	1.5	2
350	406	221	5.3	2
155	340	387	0.9	100
190	470	324	1.5	100
350	406	198	5.3	100

Table 5.
Q, UTS and %El values for alloy A after 2 and 100 h aging at different temperatures.

Heat treatment procedures and parameters			
Heat treatment	**Solution treatment**	**Quenching**	**Aging**
SHT*	495°C for 5 h	Warm water (60°C)	NA
T5 temper	N/A	N/A	180°C for 8 h
T6 temper	495°C for 5 h	Warm water (60°C)	180°C for 8 h

SHT, solution heat treatment.

Table 6.
Heat treatment procedures and parameters applied to alloys investigated in stage II.

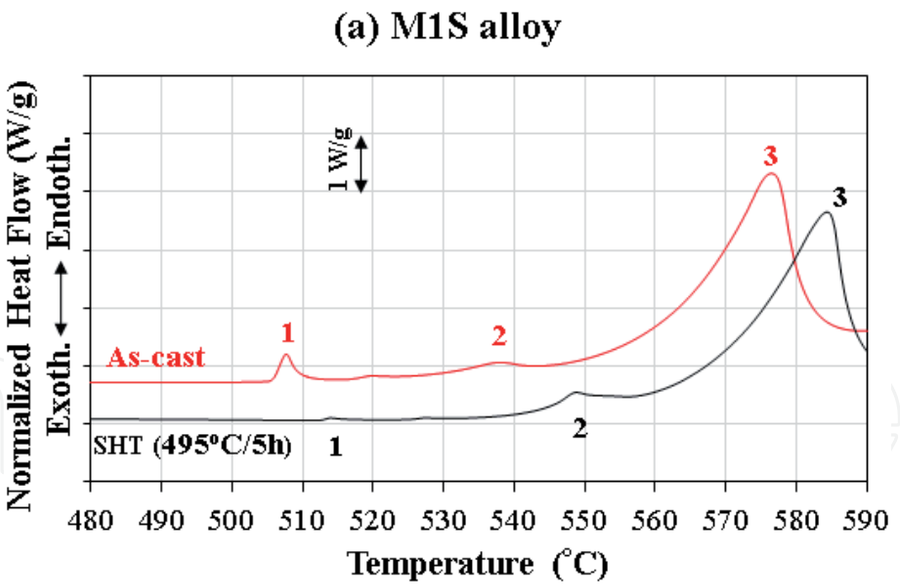

Figure 7.
Portion of the DSC heating curves of as-cast and as-quenched alloy B samples [27].

or less negligible due to dissolution of most of the Al_2Cu phase, as shown in **Figure 4(b)**.

The principle phases seen in alloy B are demonstrated in the optical as well as backscattered (BSE) images displayed in **Figure 8(a)** and **(b)** [27], respectively. **Figure 8(a)** exhibits α-Al dendrites separated by eutectic silicon colonies. The phases observed in **Figure 8(b)** were identified using EDS analysis and reference to the results of Hernandez-Sandoval [28] and Garza-Elizondo [29]. Selective EDS spectra identifying these phases are displayed in **Figure 8(c)** through **Figure 8(d)**. The existence of Al_2Cu phase in the block-like form may be attributed to the presence of Sr. in the alloy which leads to segregation of copper to localized areas [30]. The platelets of the Fe-rich β-Al_5FeSi phase are easily recognized in the BSE image, surrounded by the blocky Al_2Cu particles. The Mg-rich *Q*-phase ($Al_5Cu_2Mg_8Si_6$) is found growing out of the Al_2Cu phase as seen in the BSE image. The absence of coarse Al_3Zr precipitates [31] may be related to superheating that led to considerable dissolution of the Al_3Zr phase from the master alloy during the melting process. As a result, the coarse Zr-containing phases are rarely detected since Al_3Zr particles act as nucleation spots for these coarse phases. According to Garza-Elizondo [29], coarse Zr-rich particles may be nucleated on the undissolved Al_3Zr particles provided by the master alloy, i.e., Al-15 wt.%Zr. In the present study, superheating the melt to 800°C would significantly reduce the numbers of Al_3Zr particles in the matrix. The predicted fine zirconium trialuminide (Al_3Zr) dispersoids that may be present on a nanoscale would require a high magnification BSE image to be detected.

Figure 9(a) shows a bright-field (BF) TEM image obtained in a T6-treated sample of alloy B with the electron beam parallel to the [001] zone axis. This figure shows a high density of uniformly distributed needle-like precipitates which are oriented along <110> family of directions and aligned along the [100] planes. The length of these precipitates ranges from 50 to 150 nm, close to the reported size of θ′-Al_2Cu plates (50–100 nm long) [32, 33]. **Figure 9(b)** displays the associated selected area electron diffraction (SAED) pattern obtained from **Figure 9(a)**. The observable discrete diffraction maxima for the precipitates in SAED pattern indicate the presence of θ′-Al_2Cu, where the streaks most probably result from the presence of fine S′-Al_2CuMg particles. Computer simulation studies [34–37] on the S′-phase reflections show that they are hidden within the streaks of θ′.

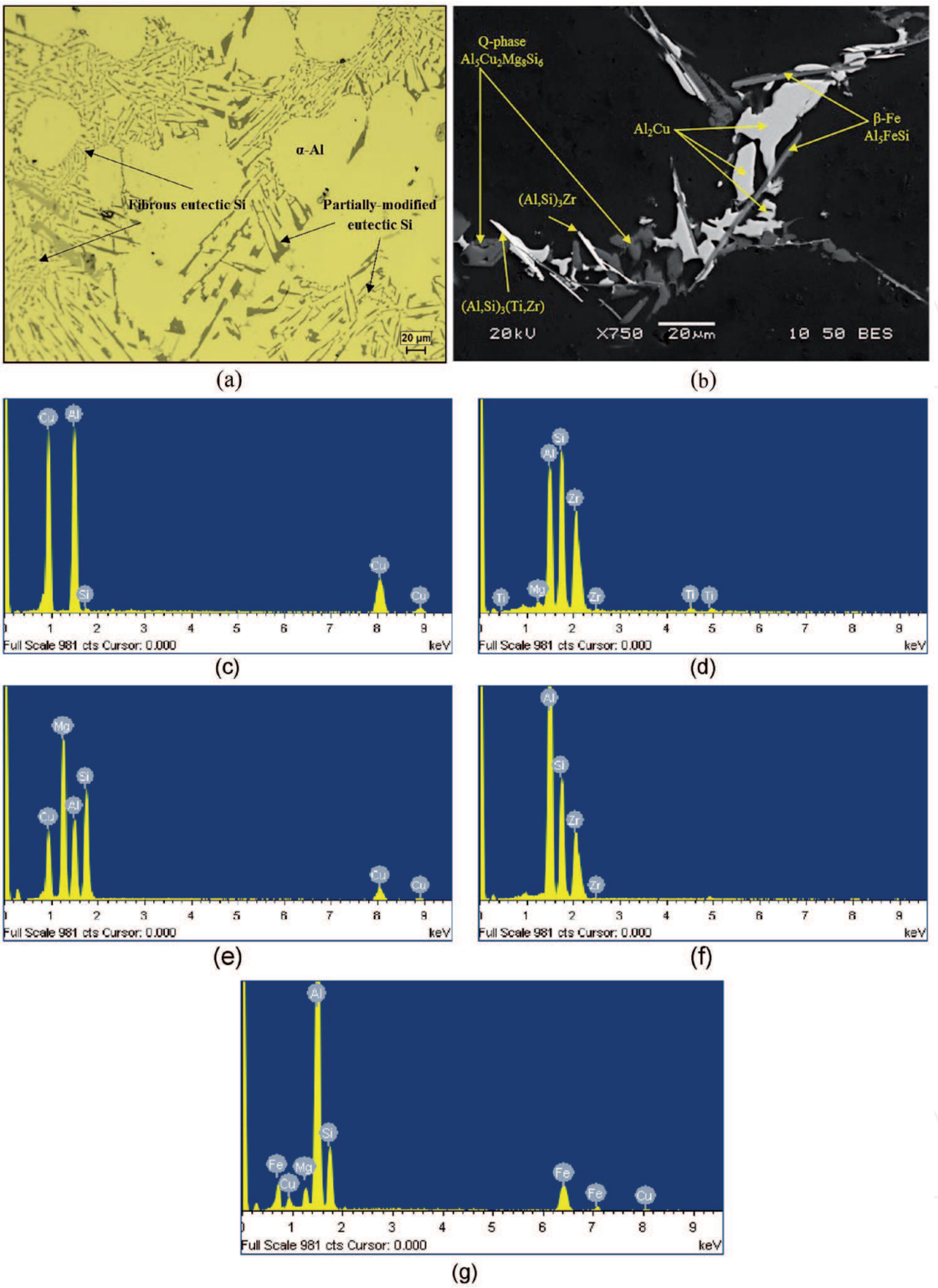

Figure 8.
(a) Optical micrograph at 200× magnification, and (b) backscattered electron image of alloy B (354 + 0.3 wt.%Zr), obtained at a low cooling rate of 0.35°C/s, showing the different phases present in the alloy; (c–g) EDS spectra corresponding to Al_2Cu, $(Al,Si)_3(Ti,Zr)$, Q-$Al_5Mg_8Cu_2Si_6$, $(Al,Si)_3Zr$, and β-Al_5FeSi phases observed in (b) [27].

In the present work, **Figure 10(a)**, the addition of ~0.3 wt.%Zr to the 354-type Al-Si-Cu-Mg cast alloy in the as-cast condition improves the ambient-temperature (25°C) strength values of the Zr-free 354 alloy (alloy A), by ~26 MPa (UTS) and 40 MPa (YS), respectively. Following SHT, the UTS and ductility values remained almost constant at ~300 MPa and ~ 6.3%, respectively, while the yield strength increased by ~33 MPa compared to alloy A. It is believed that the improved strength

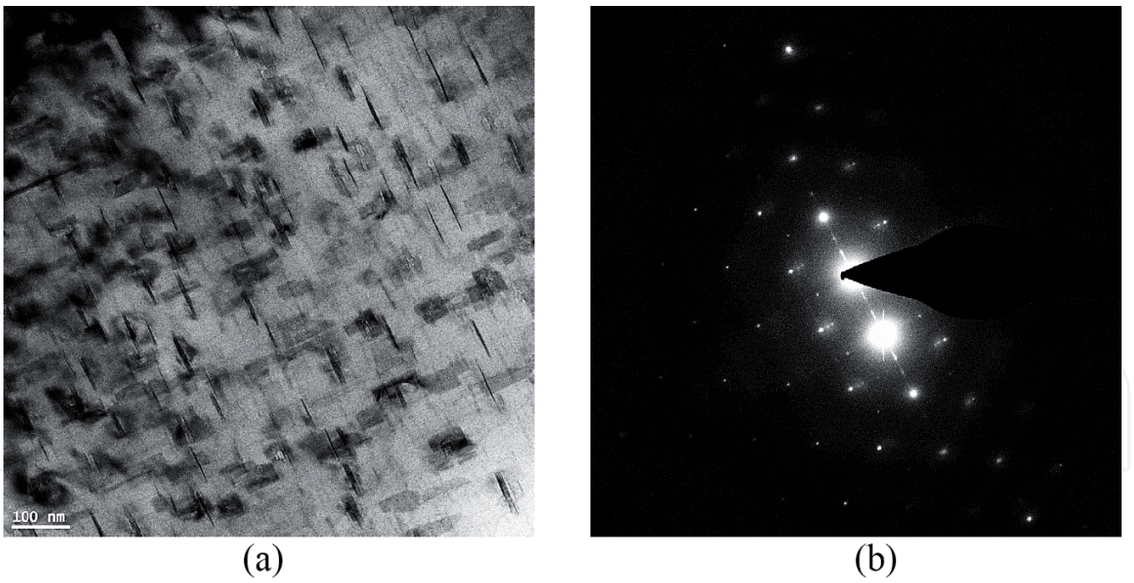

Figure 9.
(a) Bright-field TEM image of alloy B in T6-treated condition, and (b) the selected area electron diffraction (SAED) pattern.

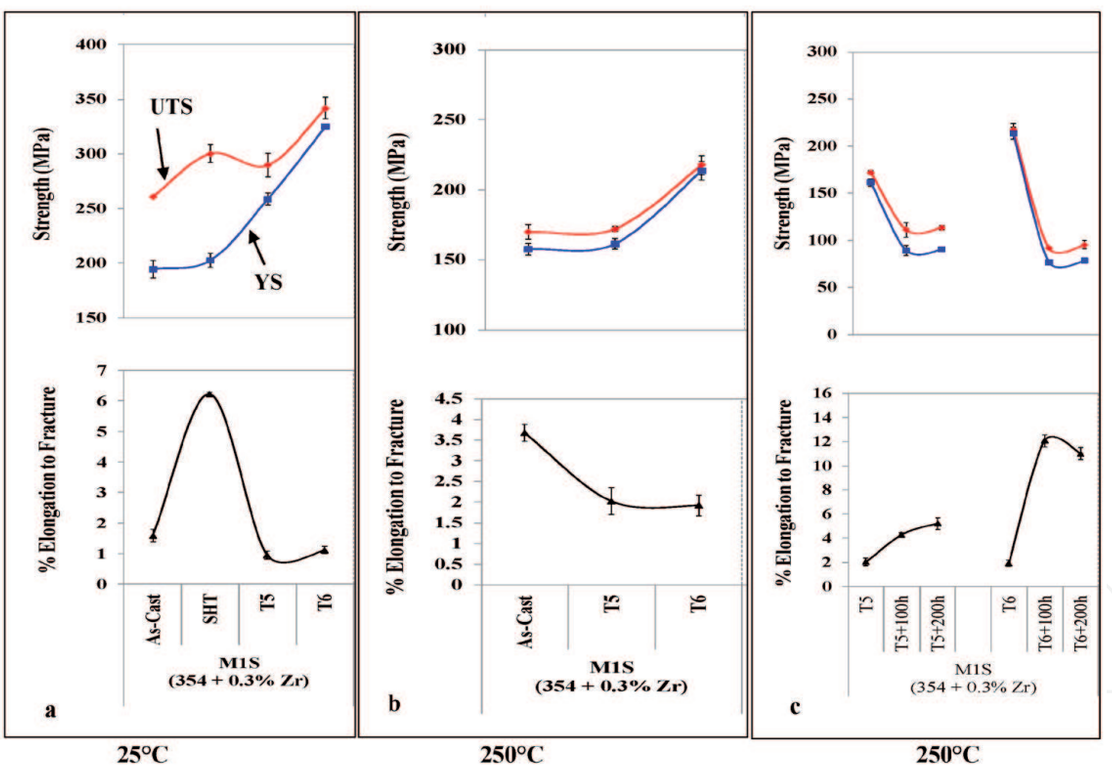

Figure 10.
(a) Ambient, and (b, c) high temperature tensile properties of alloy B.

values of alloy B emphasizes the role of Zr addition in enhancing the ambient-temperature tensile properties through the formation of fine secondary strengthening precipitates (Al_3Zr) as reported by many authors [14, 38–40]. The fact that UTS and YS in the T5 and T6 conditions are very close may be attributed to the strengthening effect of the fine dispersoids, which precipitate during the artificial aging stage of the T5, and T6 treatments as reported in **Figure 9**.

Tensile testing at 250°C, endured a significant softening due to the possible coarsening of the strengthening precipitates (Al_2Cu) that existed during tensile testing at room temperature (**Figure 11**). In addition, the T5 heat treatment did

not improve the elevated-temperature strength values of the as-cast alloys but reduced the alloy ductility by ~50%. However, application of the T6 heat treatment noticeably enhanced the strength values of the as-cast condition from about 175 to 225 MPa. Another parameter to consider is the effect of thermal stability. In the present work, some tensile samples were stabilized at 250°C (following the T5 and T6 aging treatment) for a lengthy period of time, i.e., 100 and 200 h. As can be seen from **Figure 10(c)**, the stabilized T5-treated alloy B samples exhibit better strength values (UTS and YS) than those obtained in the stabilized T6-treated condition. However, the ductility values obtained after stabilization of the T5-treated samples are dramatically lower in comparison. **Figure 11(a)** shows Al_2Cu particle size and distribution in a T6 sample stabilized at 250°C for 200 h, whereas **Figure 11(b)** is the corresponding EDS spectrum.

A detailed investigation of the fracture surfaces of tensile bars of alloy B were examined in the T6-treated condition, before and after stabilization for 200 h at 250°C. The T6-temper treatment was selected due to its wide use in the automotive industry. The BSE image shown in **Figure 12(a)** [41] shows the fracture surface of the tensile-tested alloy in the T6-treated condition. The fracture surface

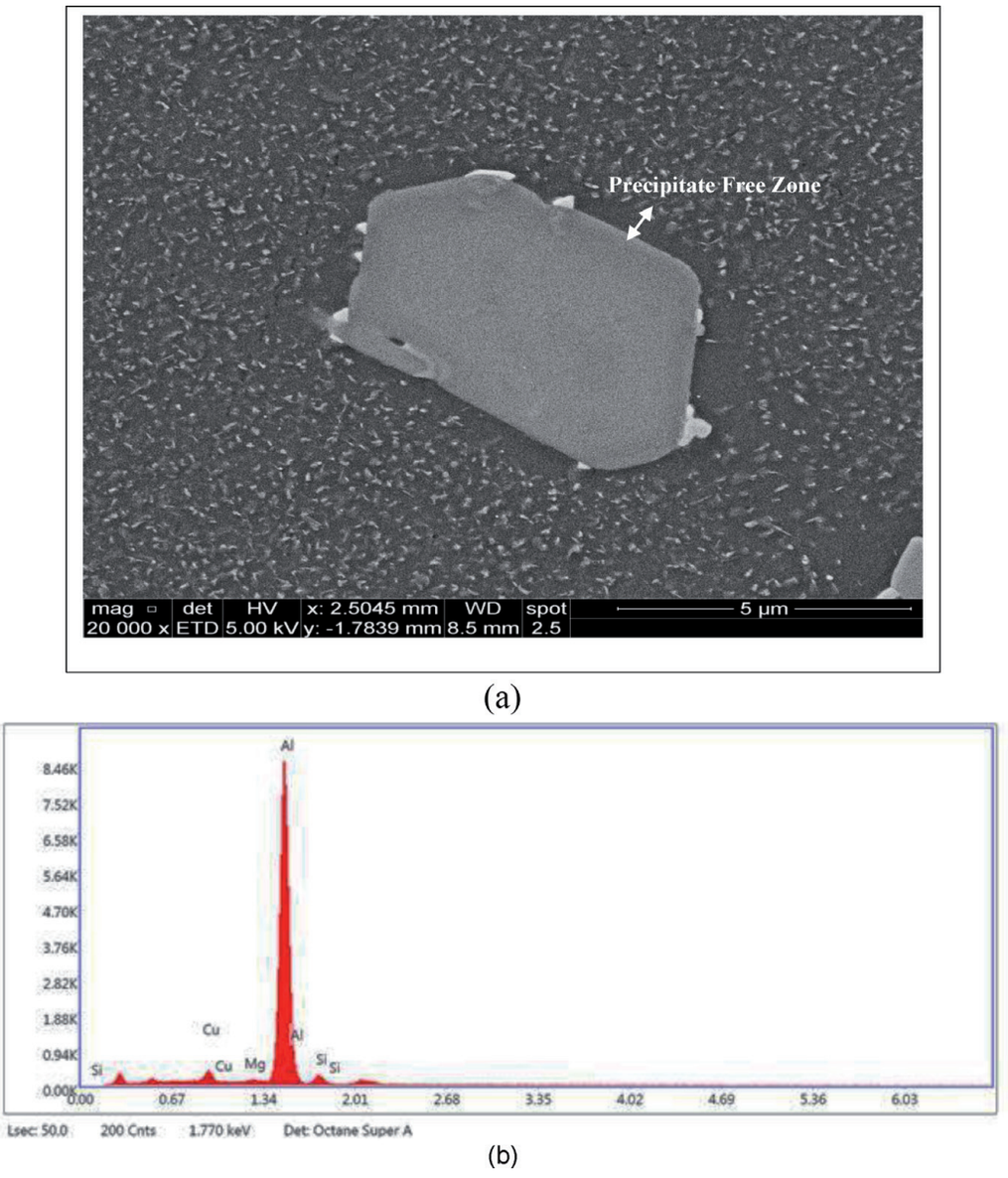

Figure 11.
(a) Backscattered electron images showing the size and distribution of precipitates in the T6-treated B alloy after stabilization at 250°C for 200 h; (b) EDS spectrum corresponding to the rod-like particles in (a).

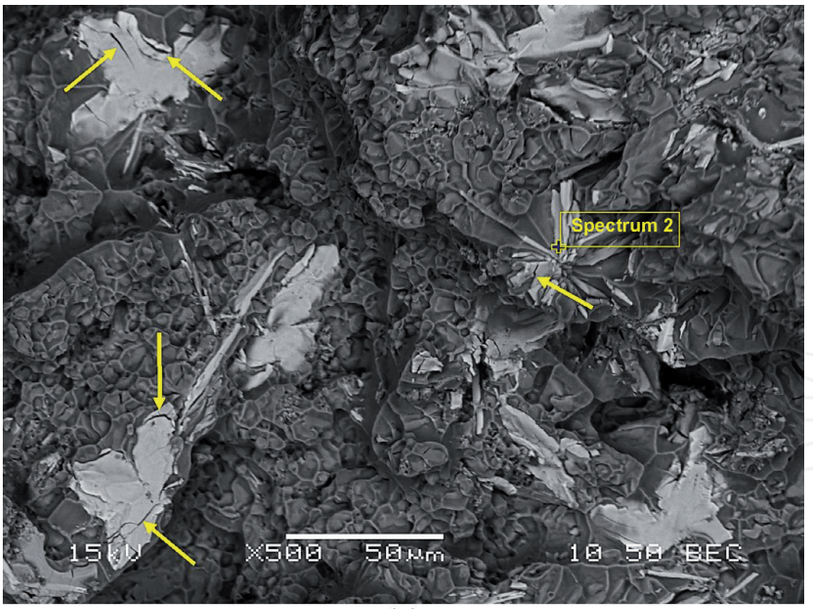

(a)

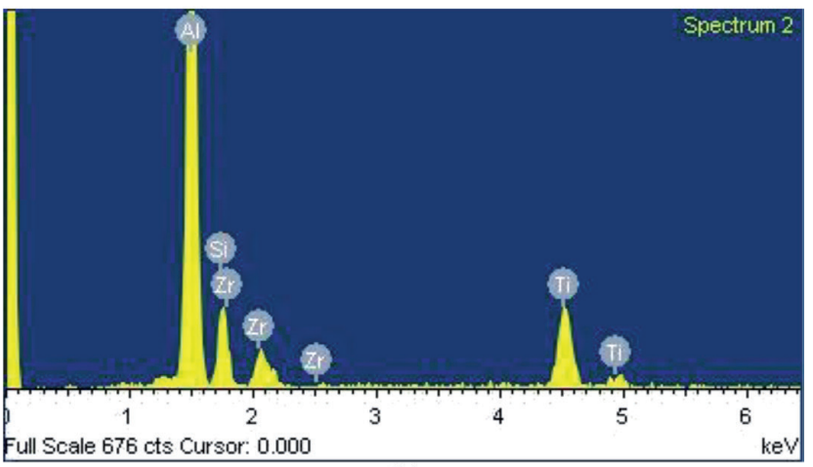

(b)

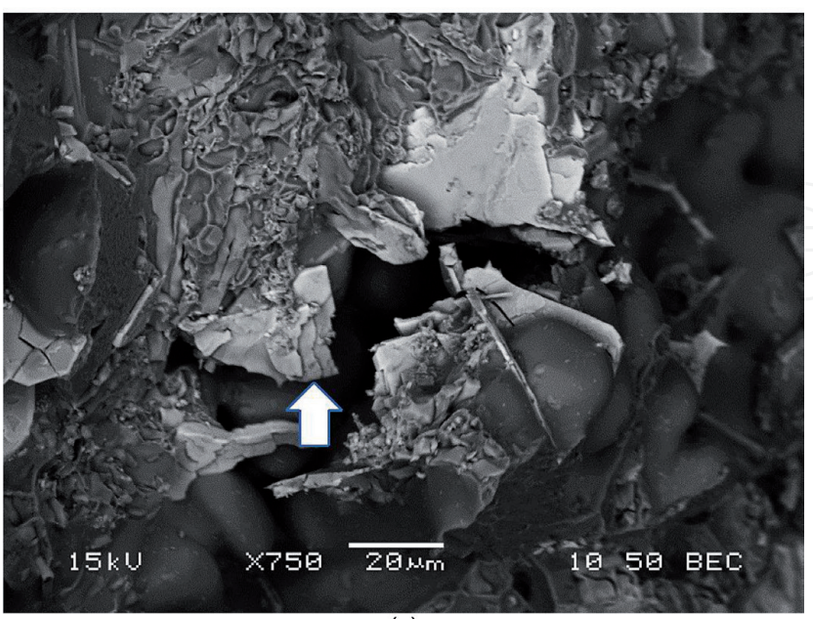

(c)

Figure 12.
Fracture surface of T6-treated alloy B: (a) BSE image showing a uniform dimple structure and cracked particles (arrowed), (b) EDS spectrum corresponding to the point of interest in (a), and (c) high magnification BSE image showing a cracked Al-Si-Ti-Zr particle (arrowed) [41].

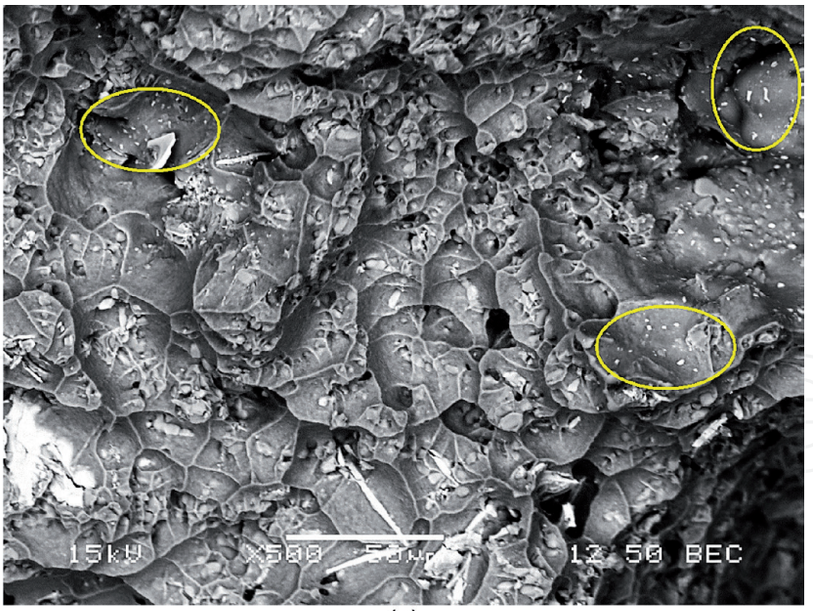

(a)

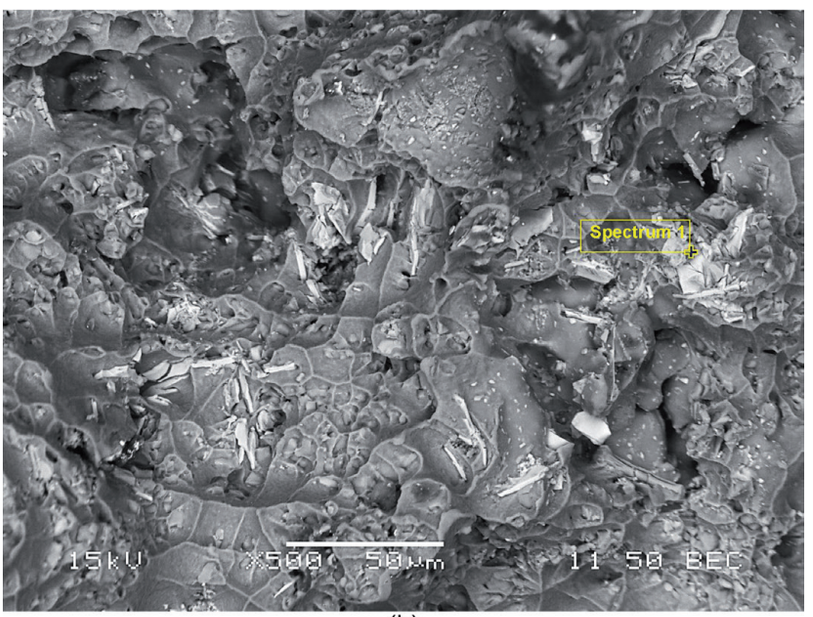

(b)

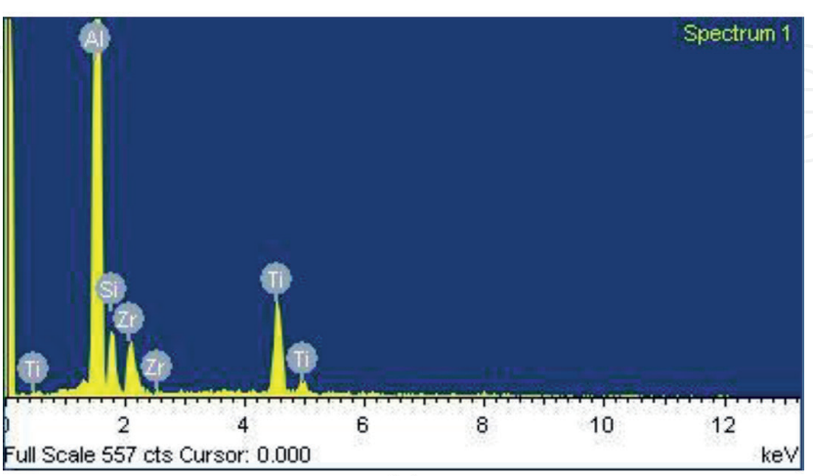

(c)

Figure 13.
Fracture surface of alloy B: (a, b) BSE images of T6-treated alloy after stabilization at 250°C for 200 h showing a coarse dimpled structure, coarsened precipitates and $Al_x(Zr,Ti)Si$ particles involved in the crack initiation process, and (c) corresponding EDS spectrum of the phase of interest as shown in (b) [41].

has a dimpled-structure throughout, which indicates the ductile nature of the fracture mode. In addition, the BSE image exhibits the precipitation of Al_x(Zr,Ti)Si compound, in the form of star-like shape, as confirmed by the associated EDS spectrum in **Figure 12(b)**. Also, cracks can be spotted in various particles of this compound, as indicated by the arrows. The higher magnification BSE image shown in **Figure 11(c)** reveals a cracked Al_x(Zr,Ti)Si phase particle.

Figure 13(a) [41] shows the fracture surface of the T6-treated B alloy tested at 250°C after stabilization for 200 h at the testing temperature. The dimple structure is coarser compared to that before stabilization at 250°C. This observation would explain the improved ductility of the alloy due to the softening behavior associated with the prolonged elevated-temperature exposure at 250°C. Coarsened precipitates appear in the interiors of the dimples, as indicated by the oval contours in **Figure 13(a)**. The BSE image and the EDS spectrum shown in **Figure 13(b)** and **(c)**, respectively, confirm the presence of Al_x(Zr,Ti)Si phase particles.

4. Conclusions

Based on an analysis of the results presented in this article, the following conclusions may be made:

1. For the base 354 alloy A, solution heat treatment and artificial aging at 190°C for 2 h or at 155°C for 100 h resulted in an increase in the alloy strength by ~64% over its as-cast strength. Aging at 155 or 170°C for a long period of time offered maximum resistance to softening.

2. The Zr-rich intermetallic phases appear in two different forms, namely $(Al,Si)_2$(Zr,Ti) in block-like form, and containing high level of silicon, and $(Al,Si)_3$(Zr,Ti) in needle-like form, containing high level of aluminum.

3. Quality index (Q) charts constructed for alloy 354 characterize the tensile properties in terms of the heat treatment conditions applied. Minimum and maximum Q values, i.e., 259 and 459 MPa, are observed for the as-cast and solution heat-treated conditions, respectively; the yield strength shows a maximum of 345 MPa and a minimum of 80 MPa within the range of aging treatments applied.

4. DSC runs carried out on alloy B (354 alloy + 0.3%Zr) revealed peak patterns which included differences in peak heights—which reflected the amount of the precipitated phase, and shifts in the transformation temperature.

5. Melt superheating at 800°C is beneficial in terms of reducing the amount of coarse Zr-rich phases in the alloy structure, as it provides efficient dissolution of the Al_3Zr phase from the master alloy during the melting process. Coarse Zr-containing phases are rarely observed due to the limited number of Al_3Zr particles available to act as nucleation sites for these coarse phases.

6. TEM investigations confirm that the investigated alloys are strengthened primarily by θ-Al_2Cu and S-Al_2CuMg precipitates and their precursors, in addition to a secondary strengthening effect by precipitates in the form of Al_x(Zr,Ti)Si which form following the addition of Zr.

7. Prolonged exposure at 250°C, resulting in coarsening of the strengthening precipitates, causes noticeable reduction in strength values, particularly the yield strength (cf. 160 and 325 MPa), and a remarkable increase in the ductility values (cf. 6.3 and 1.1%).

8. The strength values (UTS and YS) obtained at room temperature for the stabilized T5-treated alloy samples are comparable to those of the stabilized T6-treated condition, and higher in the case of elevated-temperature tensile testing.

9. The fracture surface of the T6-treated alloy B after stabilization for 1 h at 250°C reveals a dimpled-structure throughout, indicating the ductile nature of the fracture mode.

The $Al_x(Zr,Ti)_{1-x}Si$ complex compound is observed with star-like and blocky morphologies, with cracks appearing in various particles of this compound. By increasing the stabilization time up to 200 h, coarser and deeper dimples are formed, highlighting the improved ductility of the alloy due to the softening behavior associated with the prolonged exposure at 250°C.

Author details

Jacobo Hernandez-Sandoval[1,2], Mohamed H. Abdelaziz[1,3], Agnes M. Samuel[1], Herbert W. Doty[4] and Fawzy H. Samuel[1*]

1 Département des Sciences appliquées, Université du Québec à Chicoutimi, Canada

2 Facultad de Ingeniería Mecánica y Eléctrica, Universidad Autónoma de Nuevo Leon, Mexico

3 Département PEC, Université Française d'Égypte, Le Caire, Egypt

4 General Motors Global Technology Center, Warren, MI, USA

*Address all correspondence to: fhsamuel@uqac.ca

References

[1] Ibrahim MF, Samuel AM, Doty HW, Samuel FH. Effect of aging conditions on precipitation hardening in Al-Si-Mg and Al-Si-Cu-Mg alloys. International Journal of Metalcasting. 2017;**11**(2):274-286

[2] Hatch JE. Aluminum: Properties and Physical Metallurgy. USA: ASM International; 1984

[3] Samuel FH, Samuel A. Effect of heat treatment on the microstructure, tensile properties, and fracture behavior of permanent mold Al-10 Wt Pct Si-0.6 Wt Pct Mg/sic/10 P composite castings. Metallurgical and Materials Transactions A. 1994;**25**(10):2247-2263

[4] Ibrahim MF, Abdelaziz MH, Doty HW, Valtierra S, Samuel FH. Effect of microalloying elements on the heat treatment response and tensile properties of Al-Si-Mg alloys. In: Ares AE, editor. Solidification. Rijeka: IntechOpen; 2018. Ch. 01

[5] Hernandez-Sandoval J, Garza-Elizondo GH, Samuel AM, Valtierra S, Samuel FH. The ambient and high temperature deformation behavior of Al-Si-Cu-Mg alloy with minor Ti, Zr, Ni additions. Materials & Design. 2014;**58**:89-101

[6] Meyers C, Hinton K, Chou J-S. Towards the optimization of heat-treatment in aluminium alloys. Materials Science Forum. 1992;**72**:102-104

[7] Mohamed AMA, Samuel FH. A review on the heat treatment of Al-Si-Cu/Mg casting alloys. In: Czerwinsk F, editor. Heat Treatment; Conventional and Novel Applications. Rijeka: IntechOpen; 2012. Chapter 4

[8] Cayron C, Buffat P. Transmission electron microscopy study of the B′ phase (Al–Mg–Si alloys) and Qc phase (Al–Cu–Mg–Si alloys): Ordering mechanism and crystallographic structure. Acta Materialia. 2000;**48**(10):2639-2653

[9] Matsuda K, Teguri D, Sato T, Ikeno S. EFTEM observation of Q'phase in Al-Mg-Si-Cu alloy. Materials Science Forum. 2002;**396**(4):947-951

[10] Hwang J, Banerjee R, Doty H, Kaufman M. The effect of Mg on the structure and properties of type 319 aluminum casting alloys. Acta Materialia. 2009;**57**(4):1308-1317

[11] Wang G, Sun Q, Feng L, Hui L, Jing C. Influence of Cu content on ageing behavior of AlSiMgCu cast alloys. Materials & Design. 2007;**28**(3):1001-1005

[12] Abdelaziz MH. Microstructural and mechanical characterization of transition elements-containing Al-Si-Cu-Mg alloys for elevated-temperature applications [PhD thesis]. Canada: UQAC; 2018

[13] Srinivasan D, Chattopadhyay K. Metastable phase evolution and hardness of nanocrystalline Al–Si–Zr alloys. Materials Science and Engineering A. 2001;**304**:534-539

[14] Knipling KE. Development of a nanoscale precipitation-strengthened creep-resistant aluminum alloy containing trialuminide precipitates [PhD thesis]. USA: Northwestern University; 2006

[15] Ragab K. The use of fluidized sand bed as an innovative technique for heat treating aluminum based castings [PhD thesis]. Canada: UQAC; 2012

[16] Mohamed A, Samuel A, Samuel F, Doty H. Influence of additives on the microstructure and tensile properties of near-eutectic Al–10.8% Si

cast alloy. Materials & Design. 2009;**30**(10):3943-3957

[17] Drouzy M, Jacob S, Richard M. Interpretation of tensile results by means of quality index and probable yield strength-application to Al-Si7 Mg foundry alloys-France. International Journal of Cast Metals. 1980;**5**(2):43-50

[18] Jacob S. Quality index in prediction of properties of aluminum castings—A review. In: Transactions of the American Foundry Society and the One Hundred Fourth Annual Castings Congress. Vol. 208. Pittsburgh, Pennsylvania; 2000. pp. 811-818

[19] Cáceres C. A rationale for the quality index of Al-Si-Mg casting alloys. International Journal of Cast Metals Research. 2000;**12**(6):385-391

[20] Abdelaziz MH, Doty HW, Valtierra S, Samuel FH. Static versus dynamic thermal exposure of transition elements-containing Al-Si-Cu-Mg cast alloy. Materials Science and Engineering A. 2019;**739**:499-512

[21] Tahiri H, Mohamed SS, Doty HW, Valtierra S, Samuel FH. Effect of Sr–grain refining–Si interactions on the microstructural characteristics of Al–Si hypoeutectic alloys. International Journal of Metalcasting. 2018;**12**(2):343-361

[22] Zhu PY, Liu QY. Kinetics of granulation of discontinuous phase in eutectic structures. Materials Science and Technology. 1986;**2**:500-507

[23] Reif W, Dutkiewiewicz J, Ciach R. Effect of precipitates in Al-Si-Cu-Mg alloys. Materials Science and Engineering A. 1997;**234**:165-168

[24] Ammar HR, Samuel AM, Samuel FH. Porosity and the fatigue behavior of hvpoeutectic and hypereutectic aluminum-silicon casting alloys. International Journal of Fatigue. 2008;**30**(6):1024-1035

[25] Câceres CH, Taylor JA. Enhanced ductility in Al-Si-Cu-Mg casting alloys with high Si content. In: Tiryakiouglu M, Crepeau P, editors. Shape Casting: The John Campbell Symposium. California: TMS; 2005. pp. 245-254

[26] Toschi S. Optimization of A354 Al-Si-Cu-Mg alloy heat treatment: Effect on microstructure, hardness, and tensile properties of peak aged and overaged alloy. Metals. 2018;**8**:961. DOI: 10.3390/met8110961

[27] Abdelaziz MH, Elgallad EM, Doty HW, Valtierra S, Samuel FH. Melting and solidification characteristics of Zr-, Ni-, and Mn-containing 354-type Al-Si-Cu-Mg cast alloys. Philosophical Magazine. 2019;**99**(13):1633-1655

[28] Hernandez Sandoval J. Improving the Performance of 354 Type Alloy [PhD thesis]. Canada: Université du Québec à Chicoutimi; 2010

[29] Garza-Elizondo GH. Effect of Ni, Mn, Zr and Sc Additions on the Performance of Al-Si-Cu-Mg Alloys [PhD thesis]. Canada: UQAC; 2016

[30] Ibrahim MF, Samuel E, Samuel AM, Al-Ahmari AMA, Samuel FH. Metallurgical parameters controlling the microstructure and hardness of Al-Si-Cu-Mg base alloys. Materials & Design. 2011;**32**(4):2130-2142

[31] Priya P, Matthew JM, Krane JM, Johnson DR. Precipitation of Al_3Zr dispersoids during homogenization of Al-Zn-Cu-Mg-Zr alloys. In: Light Metals. 2016. pp. 213-218

[32] Tavitas-Medrano F, Gruzleski J, Samuel F, Valtierra S, Doty H. Effect of Mg and Sr-modification on the mechanical properties of 319-type aluminum cast alloys subjected to artificial aging. Materials Science and Engineering A. 2008;**480**(1):356-364

[33] Reif W, Dutkiewicz J, Ciach R, Yu S, Krol J. Effect of ageing on the evolution of precipitates in AlSiCuMg alloys. Materials Science and Engineering A. 1997;**234**:165-168

[34] Purtee M. Aging effects of an aluminum-based 319 alloy. Foundry Management & Technology. 1998;**126**(10):42-44

[35] Takeda M, Ohkubo F, Shirai T, Fukui K. Precipitation behaviour of Ai-Mg-Si ternary alloys. In: Materials Science Forum, Vol. 217-222. Stafa-Zurich, Switzerland: Trans Tech Publications, Ltd.; 1996. pp. 815-820

[36] Elwazri A, Varano R, Siciliano F, Bai D, Yue S. Characterisation of precipitation of niobium carbide using carbon extraction replicas and thin foils by FESEM. Materials Science and Technology. 2006;**22**(5):537-541

[37] Kang H, Kida M, Miyahara H, Ogi K. Age-hardening behavior of Al-Si-Cu base cast alloys. Journal of Japan Foundry Engineering Society. 1997;**69**(10):828-834

[38] Shaha SK. Development and characterization of cast modified Al-Si-Cu-Mg alloys for heat resistant power train applications [PhD thesis]. Canada: Ryerson University; 2015

[39] Knipling KE, Dunand DC, Seidman DN. Nucleation and precipitation strengthening in dilute Al-Ti and Al-Zr alloys. Metallurgical and Materials Transactions A. 2007;**38**(10):2552-2563

[40] Knipling KE, Dunand DC, Seidman DN. Precipitation evolution in Al–Zr and Al–Zr–Ti alloys during isothermal aging at 375-425 C. Acta Materialia. 2008;**56**(1):114-127

[41] Abdelaziz MH, Elgallad EM, Samuel AM, Doty HW, Samuel FH. High-temperature tensile fractography of Zr-, Ni-, and Mn-containing Al-Si-Cu-Mg cast alloys. Advances in Materials Science and Engineering. 2020